PCCP

PAPER

Cite this: *Phys. Chem. Chem. Phys.*, 2017, **19**, 19021

Direct examination of the relevance for folding, binding and electron transfer of a conserved protein folding intermediate†

Emilio Lamazares,[ab] Sonia Vega,[a] Patricia Ferreira,[ab] Milagros Medina,[ab] Juan J. Galano-Frutos,[ab] Marta Martínez-Júlvez,[ab] Adrián Velázquez-Campoy[abcd] and Javier Sancho*[abd]

Received 20th April 2017,
Accepted 3rd July 2017

DOI: 10.1039/c7cp02606d

rsc.li/pccp

Near the minimum free energy basin of proteins where the native ensemble resides, partly unfolded conformations of slightly higher energy can be significantly populated under native conditions. It has been speculated that they play roles in molecular recognition and catalysis, but they might represent contemporary features of the evolutionary process without functional relevance. Obtaining conclusive evidence on these alternatives is difficult because it requires comparing the performance of a given protein when populating and when not populating one such intermediate, in otherwise identical conditions. Wild type apoflavodoxin populates under native conditions a partly unfolded conformation (10% of molecules) whose unstructured region includes the binding sites for the FMN cofactor and for redox partner proteins. We recently engineered a thermostable variant where the intermediate is no longer detectable. Using the wild type and variant, we assess the relevance of the intermediate comparing folding kinetics, cofactor binding kinetics, cofactor affinity, X-ray structure, intrinsic dynamics, redox potential of the apoflavodoxin–cofactor complex (Fld), its affinity for partner protein FNR, and electron transfer rate within the Fld/FNR physiological complex. Our data strongly suggest the intermediate state, conserved in long-chain apoflavodoxins, is not required for the correct assembly of flavodoxin nor does it contribute to shape its electron transfer properties. This analysis can be applied to evaluate other native basin intermediates.

Introduction

As expected from Boltzmann's law and experimentally demonstrated,[1] protein molecules fluctuate under native conditions between different conformations. While the native ensemble is most stable and frequent, partly unfolded conformations of slightly higher energies appear to be common in the native basins of protein conformational landscapes. Some of those intermediates could become significantly populated[2] to the point of potentially playing important functional roles, and they have been proposed to participate in ligand recognition and binding,[3,4] allosteric regulation,[5–7] or catalysis.[8,9] A variety of experimental[10–12] and computational[13,14] techniques allow the identification and characterization of equilibrium intermediates in the native basin for which functional meanings are actively sought. These efforts are stimulated by the evidence that protein function is facilitated by conformational dynamics[13,15] and by an underlying assumption: that the presence of alternative conformations in the native basin constitutes an adaptative feature of proteins.

Attribution of adaptative value to certain characteristics of current proteins is not novel or without controversy. Two well known precedents concern the role of kinetic protein folding intermediates and of the marginal conformational stability of proteins. The initial finding of transiently accumulated protein folding intermediates was interpreted as indicative of their contributing to efficient folding, but they were later considered to act as kinetic traps slowing down the folding reaction. "After much heated debate" there is no consensus on whether they play a relevant role or they are just there.[16] In fact, while the presence of folding intermediates appears to be conserved through the evolution of certain protein families,[17] protein engineering has allowed to switch proteins between 2-state

[a] *Biocomputation and Complex Systems Physics Institute (BIFI)-Joint Units: BIFI-IQFR (CSIC) and GBsC-CSIC, Universidad de Zaragoza, Zaragoza, Spain*
[b] *Departamento de Bioquímica y Biología Molecular y Celular, Facultad de Ciencias, Universidad de Zaragoza, Zaragoza, Spain*
[c] *Fundación ARAID, Gobierno de Aragón, Spain*
[d] *Aragon Health Research Institute (IIS Aragón), Universidad de Zaragoza, Zaragoza, Spain. E-mail: jsancho@unizar.es*

† Electronic supplementary information (ESI) available: Tables S1–S4 and Fig. S1–S6. See DOI: 10.1039/c7cp02606d

and 3-state folders without apparently having compromised their foldability.[18] On the other hand, the typically low thermodynamic stability of proteins was initially interpreted as being the result of selection against more stable sequences due to an activity-stability trade-off.[19,20] However, it has been shown[21,22] that as long as a certain stability level is met, random drift pushes sequences towards marginal stabilities, which suggests marginal stability is not an adaptive property.[23,24]

Flavoproteins are a ubiquitous family of proteins carrying flavin cofactors (either FMN or FAD) that allow them to participate in many biological functions from cell apoptosis[25] or DNA repair[26] to light reception[27] and a large variety of metabolic reactions.[28,29] In most cases the flavin cofactor is non-covalently bound and its redox potentials experience significant changes upon binding, which links the energetics of the folding and binding equilibria with those of the electron transfer processes catalyzed. Flavodoxins, the first flavoproteins for which X-ray structures became available[30,31] have since constituted excellent models[32] to investigate the mutual influence exerted by the apoprotein moiety and the FMN cofactor in the shaping of function. Flavodoxins can belong to the long-chain or short-chain families (depending on whether or not they contain an extra binding loop used to recognize partner redox proteins), and can easily be split apart into the apoflavodoxin and the FMN cofactor, which readily reform the functional complex upon mixing.[32] In recent years, flavodoxin research has focused on the functional role of apoprotein dynamics, which has been proposed to contribute to FMN binding through a conformational selection mechanism,[33] to increase the affinity of the complex,[34] to modulate FMN redox potentials[33,35] and subsequent electron transfer,[33] and to modulate biological function by means of distinct solvation dynamics available to different redox states.[36]

The native landscape of long-chain apoflavodoxins, *e.g.* those from *Anabaena* PCC 7119[37] or *Helicobacter pylori*,[38] is dominated by the presence of an equilibrium intermediate that, at 25 °C, is only 1.0–1.5 kcal mol^{-1} less stable than the native conformation and represents around 10% of the apoflavodoxin molecules.[39] The structure of this apoflavodoxin intermediate has been solved.[11,37] It differs from the apoflavodoxin native conformation[40] in that around 1/3 of the polypeptide, encompassing the FMN binding loops and the long extra binding loop, is disordered (Fig. 1). In the long-chain *Azotobacter vinelandii* apoflavodoxin a partly unfolded form with a similar structure (PUF2) has been observed by hydrogen exchange analysis.[41]

Both the energetic proximity of the intermediate to the native conformation and the close correspondence between its disordered region and the protein segments in charge of binding the FMN cofactor and partner redox proteins suggest that it might play a role in either the assembly of flavodoxin or in tailoring its electron transfer properties.[37,39] However, it should be noticed that experimental evaluation of roles attributed to intermediates is not easy. A fair testing ideally requires direct comparison of the performance of the original protein that populates the native basin intermediate with that of a variant lacking such intermediate, but otherwise identical. To be able to perform such an unbiased test of the apoflavodoxin intermediate significance we have recently designed and obtained

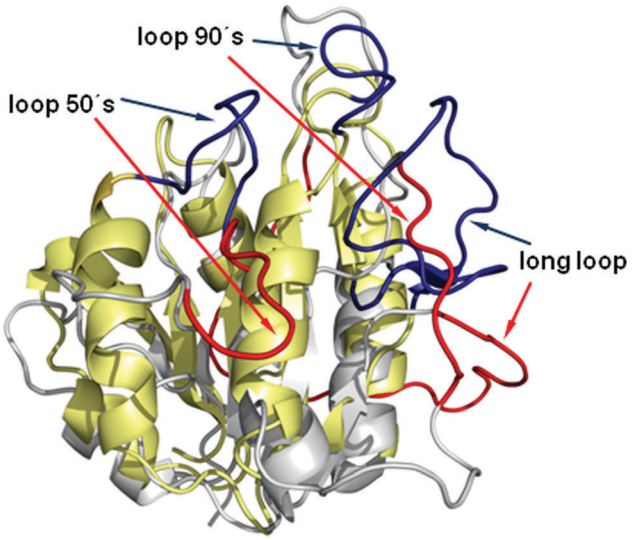

Fig. 1 Comparison of the structures of native WT apoflavodoxin (grey, pdb id 1FTG) and of the native basin thermal intermediate (sand yellow; pdb id 2KQU[37]) superimposed over residues 2–8, 18–53, 71–86, 109–117 and 153–169. Key binding loops exhibiting markedly different conformations in the two structures are highlighted in blue (native conformation) and red (intermediate), respectively.

an engineered apoflavodoxin variant (6M) containing six point mutations where the interface between the disordered and ordered regions of the intermediate has been drastically stabilized.[42]

Both differential scanning calorimetry and multiple-probe spectroscopic thermal unfolding analyses clearly indicate that this mutant, unlike its wild type precursor (WT), does not populate the partly folded intermediate but displays a simple two-state thermal unfolding.[42] We now make use of ingenuity and compare the wild type and mutant apoflavodoxin folding mechanisms, their FMN binding kinetics, their FMN affinities, the X-ray structures and intrinsic dynamics of the two flavodoxins, their resulting redox potentials, their affinities for the physiological partner enzyme ferredoxin-NADP$^+$ reductase (FNR), and the fast electron transfer efficiency within the flavodoxin/FNR complex. This comparison allows us to arrive at a surprising conclusion that, although specific to the apoflavodoxin intermediate, bears on the general assumption that intermediates at the native basin have been selected because of their adaptative value.

Results

Rationale of 6M design

The 6M flavodoxin variant was designed and built in previous work[42] by introducing in WT flavodoxin several point mutations that individually increase its lower temperature of mid denaturation (T_1) in the thermal unfolding. Four of those mutations are: I59A and I92A (replacing highly solvent exposed large hydrophobic residues by a short one), D126K (removing electrostatic repulsions[43]) and A142V (filling an internal cavity[44]). They have in common that the residues mutated appear in the locally unstable region of the native structure that becomes

unfolded in the thermal intermediate or at the interface with the stable region that remains structured. Their combined effect is to stabilize that region so that T_1 is moved upwards towards T_2 and the 3-state thermal unfolding equilibrium of WT becomes 2-state. The two additional mutations: E20K and E72K (also removing electrostatic repulsions) are located in the structured region of the WT intermediate. Their effect in the 6M mutant is to further increase its single T_m. The six mutations combined transform WT flavodoxin (T_1 = 43 °C and T_2 = 55 °C) into 6M flavodoxin (T_m = 70 °C).

Folding kinetics of the two apoflavodoxins

The folding/unfolding kinetics of WT apoflavodoxin is biphasic due to the transient accumulation of a folding intermediate that is essentially a kinetic trap in the folding pathway.[45] Although relating such kinetic intermediate with the equilibrium intermediate at the native basin observed in thermal unfolding is tempting, the correspondence between them is unclear. In fact, the folding kinetics of a shortened version of WT not populating the equilibrium intermediate was also reported as biphasic.[46] No structural information is available on the kinetic intermediate, but the structure of the transition state of apoflavodoxin unfolding, determined by ϕ-analysis and thought to be closer to the native structure, greatly differs from that of the equilibrium intermediate.[47] We have now recorded folding/unfolding kinetics of 6M apoflavodoxin, which is biphasic (Fig. 2A) and resembles that of WT, indicating the presence of a kinetic intermediate in the folding reaction of either variant. The minima of the major unfolding phases in the chevron plots of the two variants (3.8 M urea for 6M and 2.0 M urea for WT apoflavodoxin, Fig. 2B) correspond to their equilibrium urea concentrations of mid denaturation.[42,45]

Binding kinetics of the FMN cofactor to WT and 6M apoflavodoxins

Once folded, apoflavodoxin recognizes FMN molecules.[48] The binding mechanism was described for WT and mutants of binding site residues using stopped-flow kinetics followed by the quenching of FMN emission fluorescence upon binding.[49] For WT and some of the mutants analyzed the binding kinetics is monoexponential while, for some other mutants, biexponential kinetics is observed with a major fast phase accounting for 90% of the overall fluorescence change. We have now compared the binding mechanism of FMN binding to WT and 6M apoflavodoxins. The kinetics of 6M is best described by a double exponential with the fast phase representing around 80% of the global fluorescence quenching. From the slopes of k_{obs} (fast phase) *versus* [FMN] plots (Fig. 3A) k_{on} kinetic association constants of 1.08 (±0.02), and 0.19 (±0.01) ($\times 10^5$ s^{-1} M^{-1}) are estimated for the WT and 6M binding processes, respectively. 6M appears to bind FMN more slowly than WT.

Affinity of the FMN cofactor for the two apoflavodoxins

The extent to which these facts affect the strength of the functional apoflavodoxin–FMN complex (known as holoflavodoxin or simply flavodoxin) has been directly evaluated by measuring the equilibrium association constants by steady-state fluorescence titration, following the quenching of FMN emission upon binding to the apoprotein. K_b values of 1.1 (±0.5) × 10^9 M and 8.3 (±0.6) × 10^7 M have been obtained for the WT and 6M complexes, respectively. The lower affinity of the 6M complex can be visually noticed in the less sharp end of the quenching at the higher apoflavodoxin concentrations (Fig. 3B). In terms of binding energy, the 6M complex is 1.5 kcal mol^{-1} less stable than the WT one, which seems to arise from accumulation of smaller destabilizations brought about by the individual mutations present in 6M (*i.e.* a triple mutant carrying mutations E20K/E72K/D126K is 0.5 kcal mol^{-1} less stable than WT (Fig. S1A, ESI†) and double mutant I92A/I59A is 0.6 kcal mol^{-1} less stable[50]).

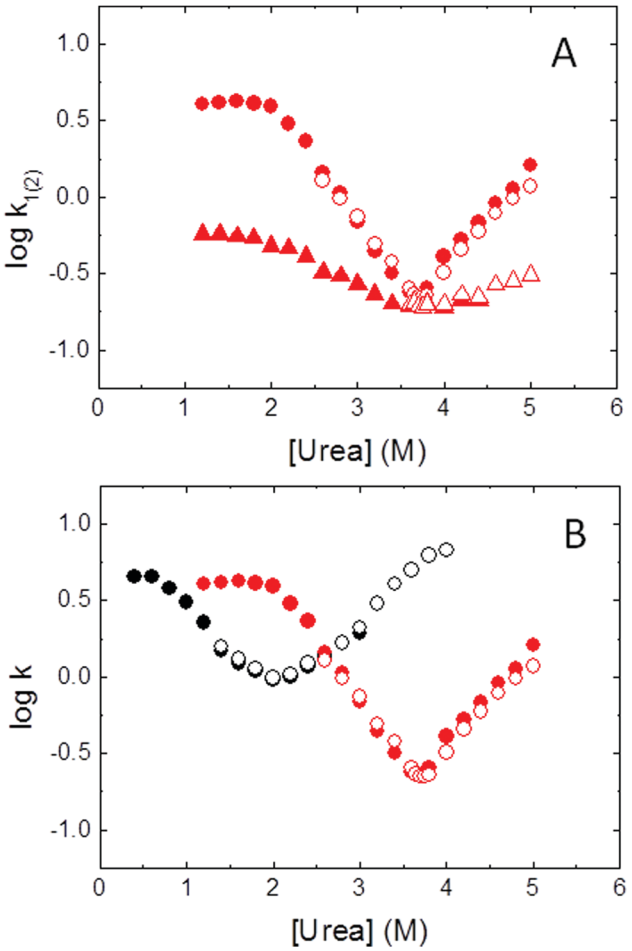

Fig. 2 Chevron plots of WT and 6M apoflavodoxin folding and unfolding kinetics. (A) Characterization of 6M apoflavodoxin folding/unfolding kinetics. Urea dependence of the observed folding (filled red circles: fast phase; filled red triangles: slow phase) and unfolding (open red circles: fast phase; open red triangles: slow phase) relaxations (determined in units of s^{-1}). (B) Comparison of the fast folding/unfolding phase of WT (filled black circles, folding; open black circles, unfolding) and 6M (filled red circles, folding; open red circles, unfolding) apoflavodoxins.

Thermostability of the two holoflavodoxins

The thermal unfolding of WT holoflavodoxin is characterized by the coupling of FMN dissociation and polypeptide unfolding,

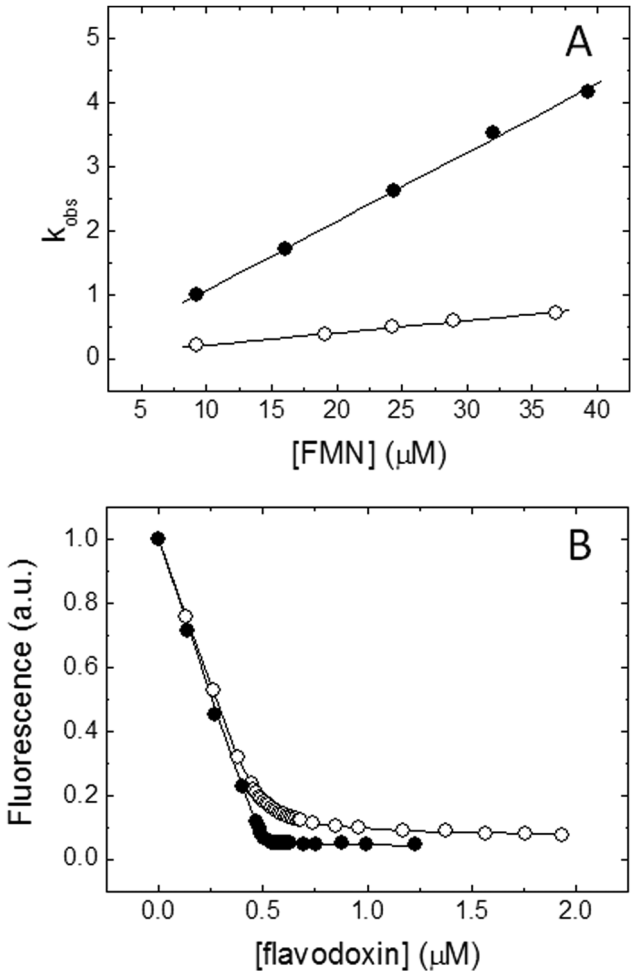

Fig. 3 (A) Secondary plots used to calculate k_{on} for FMN binding to WT and 6M apoflavodoxins from linear fits (solid lines) of the observed kinetic binding constants (k_{obs}) at different concentrations of FMN (WT: solid circles; 6M: open circles). (B) Titrations of FMN binding to WT and 6M apoflavodoxins by following the quenching of emission fluorescence at 525 nm (WT: solid circles; 6M: open circles). The fits are represented by lines. The buffer used was 50 mM MOPS, pH 7.0, and the temperature 25 °C. The titration was performed by injecting small volume apoflavodoxin aliquots into a 0.5 μM FMN solution.

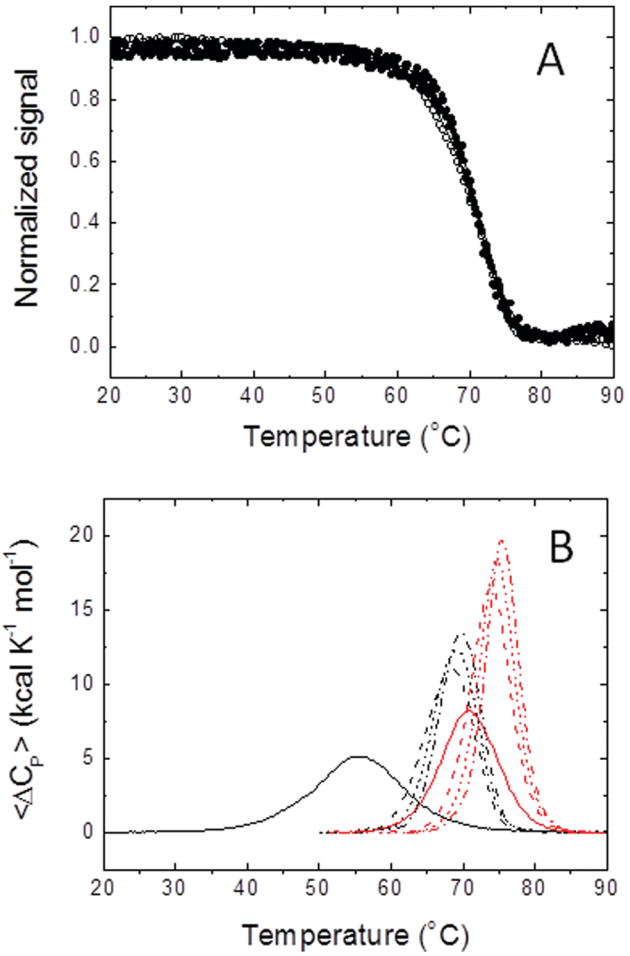

Fig. 4 (A) Thermal unfolding of 6M flavodoxin (1 : 1 apoprotein : FMN molar ratio) monitored by near-UV CD (open circles) and visible fluorescence emission (closed circles). The curves are shown normalized from 0 to 1, and their global fit to a two-state unfolding model is represented by the continuous line. (B) Differential scanning calorimetry of WT (black) or 6M (red) (apo)flavodoxins in the absence of FMN (continuous lines) or in the presence of FMN at molar ratios of 1 : 1, 1 : 2 and 1 : 3 (dashed lines of increasing T_m values, respectively). In the absence of ligand, WT apoflavodoxin exhibits a single apparent peak centered at 55 °C corresponding to two largely overlapping transitions. In the presence of cofactor the narrower peaks correspond to single cooperative transitions. Whether in the absence or the presence of FMN (red continuous or red dashes lines, respectively), 6M (apo)flavodoxin exhibits two-state unfolding.

and takes place in a highly cooperative manner, *i.e.* the equilibrium intermediate observed for the apo form does not populate.[48] The non covalent nature of the WT complex makes the conformational stability of the holoprotein depend on the total [FMN] so that excess free FMN increases the overall stability determined from thermal unfolding. We have now tested whether the same model applies to 6M. Thermal unfolding of an equimolar 6M/FMN solution was followed by FMN fluorescence emission and far UV CD and gave rise to superimposable curves (Fig. 4A), as reported for WT.[48] The thermal unfolding of 6M was then analyzed by DSC at different FMN concentrations (Table S1, ESI† and Fig. 4B). As the concentration of FMN increases the denaturation temperature also increases. The ratio of the $\Delta H_{VH}/\Delta H_{cal}$ data is also consistent with a two state transition (coupled to ligand dissociation; see Table S1, ESI† legend). All the thermal unfolding and FMN affinity data gathered for 6M, as that for WT, can be globally mapped into a ligand concentration/temperature phase diagram[51] (Fig. S2, ESI†) where the lack of a thermal intermediate in 6M is evidenced.

Midpoint reduction potentials

Flavodoxins can exchange electrons with partner proteins thanks to the redox activity of the FMN cofactor.[32] Unlike when it is free in solution, FMN bound to apoflavodoxin can accept electrons one by one to become first semireduced (semiquinone FMN) and then fully reduced (hydroquinone FMN). We have determined the midpoint reduction potentials for the oxidized/semiquinone and semiquinone/hydroquinone couples of

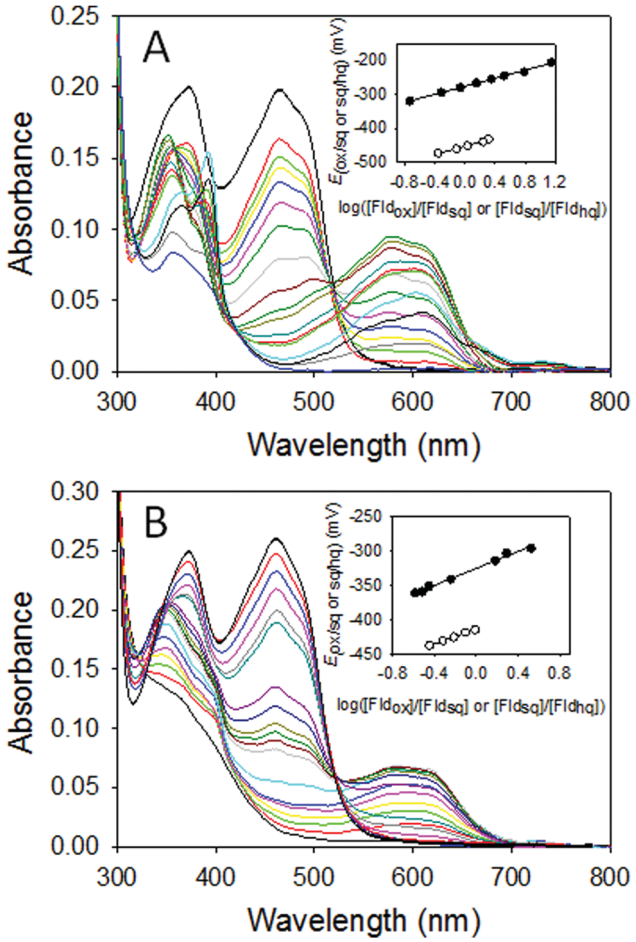

Fig. 5 Redox potentials of WT and 6M flavodoxins. UV-visible spectra of WT (A) and 6M flavodoxin (B) result of photoreduction. Insets show Nernst plots for the midpoint potential ($E_{ox/sq}$ (fill circle or squares) and $E_{sq/hq}$ (open circle or squares)) of each protein. The full oxidized form is represented by the black line in both cases.

6M flavodoxin as described[50] and compared them with those of WT (newly determined). The visible absorbance spectra of WT and 6M flavodoxins at different extents of photoreduction (Fig. 5A and B) are similar. One noticeable difference is that less 6M semiquinone (characterized by the peak at 580 nm) is stabilized during reduction than for the WT protein. The Nernst plots (insets in Fig. 5) indicate that the midpoint reduction potentials of 6M flavodoxin are 50 mV more negative ($\Delta E_{ox/sq} = -50$ mV) and 39 mV less negative ($\Delta E_{sq/hq} = +39$ mV) (Table S2, ESI†) than those of WT, which explains the lower accumulation of semiquinone in 6M. These differences in redox potentials are not large. In fact, larger differences have been observed in flavodoxin variants carrying one or two of the mutations present in 6M and being fully functional in their interactions with both FNR and PSI.[52]

Affinity of the 1 : 1 flavodoxin complexes with FNR

In some cyanobacteria, flavodoxin expression is induced under iron deficiency conditions to replace iron containing ferredoxin in photosynthetic reactions, *e.g.* electron transport from PSI to ferredoxin-NADP$^+$ reductase (FNR), the enzyme that reduces NADP$^+$ to NADPH.[32] When that reaction is mediated by flavodoxin, a binary Fld:FNR complex is formed.[53] We have use ITC to determine[54] the affinity of the complexes established by FNR with WT and 6M flavodoxins (Fig. S3, ESI†) and found very similar values of the association constant K_b (2.0×10^5 and 1.9×10^5 M^{-1}, respectively; Table S3, ESI†). Although these affinities might suggest that the two complexes are similarly appropriate for efficient electron transfer, apoflavodoxin was previously reported to form a similarly tight, but obviously non-functional, complex with FNR.[54] Thus, whether efficient electron transfer can take place between 6M flavodoxin and FNR must be tested.

Electron transfer kinetics between FNR_{hq} and Fld_{ox}

In most cyanobacteria growing under low iron conditions the flavodoxin semiquinone/hydroquinone couple (Fld_{sq}/Fld_{hq}) replaces one-electron transferring ferredoxin as donor to oxidized FNR (FNR_{ox}).[55] The fast electron transfer reaction between the two proteins can be measured by stopped-flow techniques under anaerobic conditions.[56] While reaction between FNR_{ox} and WT Fld_{hq} occurs mainly within the dead time, the reverse reaction can be fully observed. To compare the efficiency of the electron transfer between FNR and either WT or 6M flavodoxin we have mixed anaerobic solutions of FNR_{hq} and Fld_{ox} and analyzed the concomitant spectral changes by spectral deconvolution, as described.[57]

Upon mixing, an initial bleaching and displacement of the maximum at 464 nm (Fld_{ox}) to 458 nm (characteristic of FNR_{ox}) occurred; then a neutral semiquinone band (578 nm) appeared (Fig. 6A and B). The time dependence of the evolution of the three species found is shown (insets in Fig. 5A and B). The more noticeable difference in the electron transfer kinetics refers to a lower amount of 6M semiquinone stabilized (see the height of the 578 nm maximum) compared to WT. Importantly, the electron transfer rate constants calculated from global analysis of the kinetic spectral data are very similar: (k_{obs} = 1.44 (±0.31) and 1.08 ± (0.06) s^{-1} for WT and 6M, respectively). Moreover, direct determination of semiquinone formation can be obtained from fitting of absorbance changes at 600 nm over time (Fig. S4, ESI†), which provides for the WT and 6M rate constant values of 1.41 (±0.18) and 1.38 (±0.05) s^{-1}, respectively.

X-ray structure of 6M flavodoxin

To allow the structural comparison of WT and 6M flavodoxins, we have solved the X-ray structure of the latter at 1.1 Å resolution (Fig. 7). Overall, the structure is very similar to that of WT (r.m.s.d. 0.39 Å for 167 Cα). The largest local structural difference with WT (2.49 Å for 4 Cα) appears in the 134–137 segment of the stabilized long loop (Fig. S5A and B, ESI†), which adopts an alternative conformation where a polar contact between N135 and Y119 side chains is lost and new interactions between R134 side chain and residues 131 and 133 are established. Another noticeable difference is observed in the H-bonds network at the binding site of the FMN phosphate. In 6M, residue K14 appears H-bonded to the O1P atom of FMN and more exposed

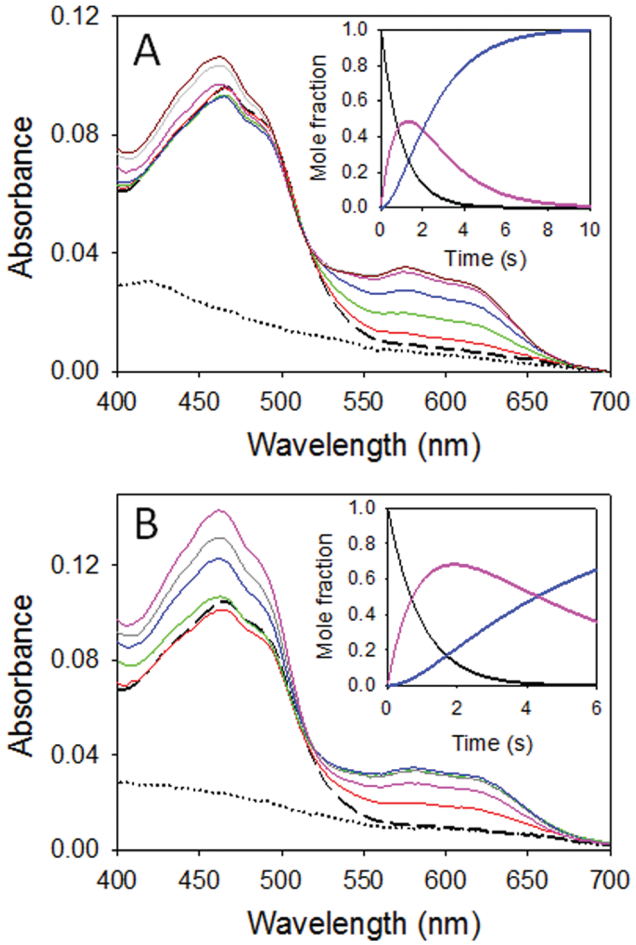

Fig. 6 Anaerobic reduction of WT Fld_{ox} (A) and its 6M variant (B) by FNR_{hq}. The spectrum of FNR_{hq} before mixing is shown as a dotted line and the first spectrum after mixing as a dashed line. Spectra after mixing are shown at 0.02, 0.12, 0.42, 1.00, 2.42, 4.50 and 7.50 seconds in (C), and at 0.02, 0.32, 1.51, 2.70, 3.61 and 5.70 seconds in (D). The insets show the evolution of the three kinetically distinguishable species obtained by global analysis of the reactions to a two steps (A → B → C) model; A (black), B (pink) and C (blue).

to solvent due to its interaction with the OD1 atom of D146 (Fig. S5C, ESI†). As a result, the FMN phosphate group is less exposed to solvent in 6M than in WT (Fig. S5D, ESI†). A further difference concerns internal packing. WT flavodoxin contains six small cavities. In 6M flavodoxin four of them shrink and two disappear (Fig. S5E, ESI†). The combined cavity volume lost mounts to 67 $Å^3$. That 6M flavodoxin is slightly more compact than WT is confirmed by direct calculation of its normalized molecular volume (see Methods), 82 $Å^3$ smaller than that of WT.

Molecular dynamics of WT and 6M flavodoxins

The higher stability of 6M relative to WT flavodoxin and its slightly tighter packing could influence its native state dynamics. To evaluate this possibility we have run five 200 ns MD simulations of each of the two flavodoxins from which we have calculated their corresponding *B*-factors. They are close to identical (Fig. 8) indicating that, in their final functional form, the two proteins explore, within the short time span simulated, the same

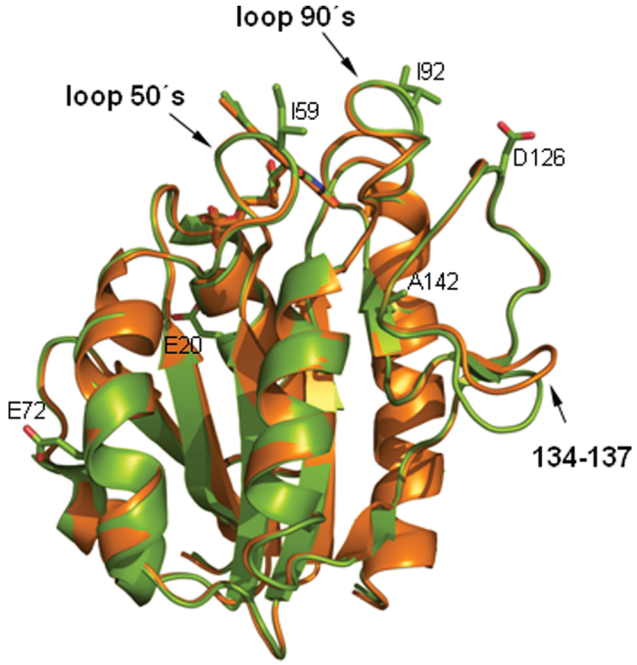

Fig. 7 Comparison of the structures of 6M (orange; pdb id 5LJP) and WT (green, pdb id: 1FLV) holoflavodoxins. Key loops are labeled. Residues shown in sticks are those mutated in the more stable 6M flavodoxin variant.

conformational space. The slightly smaller normalized volume of 6M and of its cavities relative to WT observed in the X-ray structures is also observed in averages of randomly selected frames of the trajectories (not shown).

Discussion

There is no better way to test whether an object feature is relevant than to eliminate it and compare the performance of the new object with that of the original one. The WT apoflavodoxin equilibrium intermediate populates up to 10% under native conditions and differs from the native conformation in that around one third of the polypeptide is disordered.[39] The disordered regions (Fig. 1 and 9) include segments of the protein used to bind the FMN cofactor (50's and 90's loops) and physiological partner proteins, such as the enzyme FNR (extra long loop). The presence of this intermediate in the native basin makes the thermal unfolding of apoflavodoxin a three-state process with two distinct T_ms separated by around 10 °C.[11] In a previous exercise of rational thermostabilization we engineered an apoflavodoxin variant containing 6 point mutations (6M apoflavodoxin) where the interface between the folded and disordered regions is so drastically stabilized that the intermediate can no longer be observed under thermal denaturation, and a single cooperative unfolding transition is observed at a higher temperature.[42] This indicates that the thermal intermediate is so severely destabilized in 6M that it no longer constitutes a prominent feature of the native basin.

In a wide sense the function of a polypeptide (*e.g.* its catalytic, regulatory or architectural role) relies on the overall

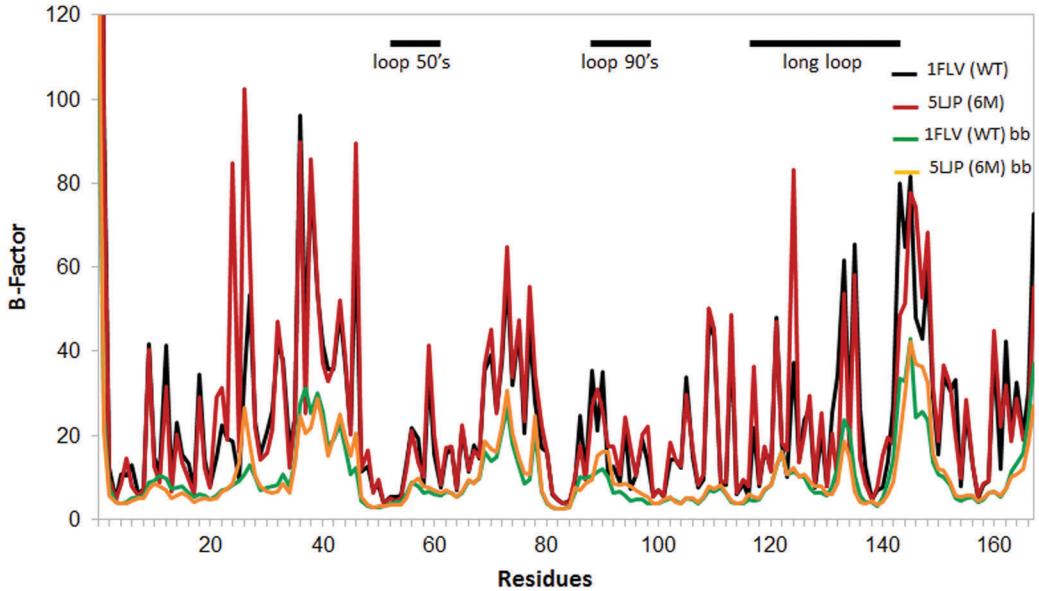

Fig. 8 Comparison of residue *B*-factors and backbone only (bb) *B*-factors in WT and 6M flavodoxins determined as their averages from five 200 ns-long MD simulations of the corresponding crystal structures (pdb ids: 1FLV and 5LJP, respectively). The location of the 50's, 90's and long extra loops is indicated.

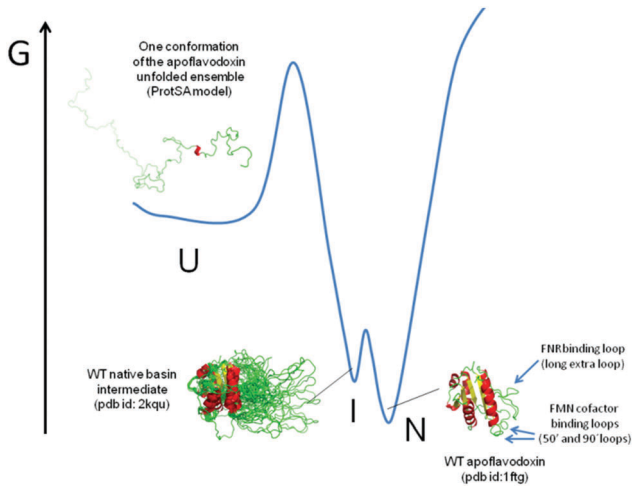

Fig. 9 Folding free energy diagram of WT apoflavodoxin showing the three relevant conformational species: the unfolded conformation (represented by one of the structures in the unfolded ensemble, as calculated with the PROTSA server[58]), the native basin intermediate constituting 10% of the molecules under native conditions (10 NMR models are shown superimposed), and the native conformation. The cofactor binding loops and the long loop used by the native protein for binding redox partner proteins such as ferredoxin $NADP^+$ reductase (FNR) are indicated by arrows. Those loops adopt disordered conformations in the native basin intermediate. In contrast, in the thermostabilized 6M apoflavodoxin no native basin intermediate is detected. Accordingly, the unfolding equilibrium of 6M apoflavodoxin is two-state.

efficiency of the several processes it experiences in order to arrive to the functional conformation. Such processes may include folding, binding, modulation of important cofactor properties or the capability to engage in additional recognition equilibria.[32] To assess the relevance of the native basin intermediate present in WT and absent in 6M apoflavodoxin in the pathway leading to the functional protein we have carefully compared the performance of the two variants. It should be expected that, if this intermediate played an important role at any point in the pathway, the assembly of 6M flavodoxin would be severely impaired relative to that of its WT precursor and, in the end, 6M flavodoxin could not efficiently participate in electron transfer reactions.

We have first compared the folding mechanisms. Both polypeptides fold through a three-state process and give rise to quite similar chevron plots (Fig. 2). Based on this similarity and on the previous quantitative analysis of the WT folding reaction[45] we can qualitatively estimate that the folding takes place at similar speed while the unfolding of the 6M mutant is around 30 times slower than that of the WT. Thus, 6M very likely folds into its native conformation by the same mechanism than WT and unfolds more slowly, as expected from its larger conformational stability. After folding, apoflavodoxin binds the FMN cofactor.[48] FMN binding to 6M apoflavodoxin is 6 times slower than to the WT protein (Fig. 3A), and gives rise to a complex that is 1.5 kcal mol^{-1} weaker (Fig. 3B). In spite of this, the thermostability of the 6M complex is still higher than that of the WT one, and the thermal unfolding of either complex follows the same two-state mechanism (Fig. 4 and Table S1, ESI†). Flavoproteins typically use apoprotein–cofactor interactions to tailor the cofactor redox potentials to their specific needs. In the case of *Anabaena* flavodoxin, the redox potentials of free FMN are unsuitable to efficiently transfer low potential electrons one by one, as required. It is the different binding affinity of apoflavodoxin for each of the three FMN redox forms[59] what greatly stabilizes the semireduced FMN form allowing it to shuttle electrons between photosystem I and the $NADP^+$ reducing enzyme FNR. This tailoring effect is evident in both WT and 6M flavodoxin redox potentials (Table S2, ESI†),

although it is less marked in 6M where the two potentials are closer to each other than in WT. As a consequence, the maximal accumulation of semireduced FMN, which takes place at similar solution potentials in either variant ($(E_1 + E_2)/2 = -364$ in WT and -369 mV in 6M) is slightly lower in 6M flavodoxin (72%) than in WT (92%) (Fig. 5). The *Anabaena* flavodoxin physiological reaction consists in transferring electrons to FNR so that this enzyme can synthesize NADPH to be used in biosynthetic reactions.[32] To that end, flavodoxin must form a 1:1 complex with FNR. Although the structure of the Fld:FNR complex has not been determined, chemical shift perturbation analysis revealed[60] that the FNR binding site extensively overlaps with the regions that appear disordered in the apoflavodoxin intermediate. The affinity of the WT and 6M complexes with FNR is quite similar (Fig. S3 and Table S3, ESI†) suggesting the two flavodoxins form similar electron-transfer complexes. Nevertheless, the electron transfer efficiency of such complexes is dependent on the precise orientation of the two proteins and of their cofactors, and is also sensitive to changes in the cofactors redox potentials.[61] We have thus directly determined the electron transfer efficiency of the WT and 6M apoflavodoxin complexes with FNR. Both complexes exchange electrons at similar rates (Fig. 6 and Fig. S3, ESI†).

The above comparison of these two cyanobacterial flavodoxin variants reveals differences in some of the properties analyzed that, except for the high thermostability and the lack of intermediate state in the native basin of 6M, are not remarkable compared to differences found between WT and many other flavodoxin mutants previously analyzed. Essentially, 6M unfolds more slowly, binds FMN more slowly and stabilizes less the FMN semiquinone redox state. Structurally, the two flavodoxins exhibit minor differences concerning a slightly tighter packing in 6M (Fig. 7 and Fig. S4, ESI†), and their intrinsic dynamics in the short time scale analyzed are very similar (Fig. 8). That any of those differences has an impact in the biological performance of the protein is far from obvious. The two apoflavodoxins fold similarly fast (Fig. 2) and the folded apoproteins are highly soluble due to their high negative charge at neutral pH. The fact is that the 6M variant is typically recovered from *E. coli* cultures as the fully functional complex carrying FMN in the semireduced state (not shown). Therefore, the slower FMN binding by 6M is not detrimental to its *in vivo* assembly into the functional complex. On the other hand, the lower stabilization of the 6M semiquinone does not seem to be detrimental either. 6M semiquinone accumulation is still high and occurs at the same redox potential than in WT, allowing electron transfer with the physiological FNR partner at a similar rate. Therefore, we must arrive to the conclusion that the apoflavodoxin equilibrium intermediate constituting 10% of the WT molecules under native conditions and having disordered FMN and FNR binding sites plays no role in allowing the folding and assembly of the holoprotein nor in shaping its capability to transfer electrons to its physiological partner. Because equivalent native basin intermediates have been described for epsilon and gamma proteobacterial apoflavodoxins (*H. pylori* I1[38] and *A. vinelandii* PUF2[41]) it is clear that populating a native basin intermediate in the apo form is a characteristic feature that has been conserved in the evolution of long-chain flavodoxins, and yet it seems to provide no adaptative value in as much as we have been able to test. Certainly, one case analysis does not allow drawing general conclusions and we cannot anticipate from this work whether the lack of adaptative value found for the apoflavodoxin intermediate will also apply to other native basin intermediates when subjected to close evaluation. Yet, our analysis challenges the widespread assumption that protein intermediates that become significantly populated under native conditions constitute adaptative features of proteins likely to play functional or other essential roles. Our results on the apoflavodoxin intermediate invite to subject native basin intermediates of other proteins to the stringent test here devised in order to substantiate claims of their roles.

Methods

Proteins

Wild type (WT) and thermostable flavodoxins 3M: (E20K/E72K/D126K) and 6M: (E20K/I59A/E72K/I92A/D126K/A142V) were obtained as previously described,[42,62] and the corresponding apoflavodoxins were prepared by removing the FMN cofactor by TCA precipitation.[62] The mutant 3M[42] is an intermediate step in the design of 6M flavodoxin, and it has also been characterized for comparison. Its data are presented in Fig. S1 (ESI†). Wild type ferredoxin $NADP^+$ reductase (FNR) was obtained as previously described.[63]

Circular dichroism (CD) spectra

Near-UV (260–310 nm) and far-UV CD (190–250 nm) spectra of the apoflavodoxin variants were recorded at 25.0 ± 0.1 °C in a Chirascan from Applied Photophysics (AP), using 20 μM protein solutions in either 50 mM MOPS buffer pH 7.0 with a 1 cm path length cuvette or 5 mM buffer plus 15 mM NaCl with a 1 mm cuvette, respectively. Near and far-UV CD spectra of the different variants are shown in Fig. S6 (ESI†).

Unfolding/refolding kinetics by stopped flow

Unfolding kinetics of apoflavodoxin solutions (40 μM in 50 mM MOPS pH 7.0) in equally buffered urea solutions were performed at 25 °C on an AP stopped-flow apparatus (DX.17 MV model) and followed by fluorescence emission (ex. at 280 nm and em. >320 nm), essentially as described.[45] Refolding kinetics were performed in a similar manner by mixing urea-unfolded apoflavodoxin (in 4.0, 5.6 or 5.8 M urea for the WT, 3M or 6M, respectively) with buffer. Unfolding/refolding kinetics was triggered by mixing 1 vol. of protein solution with 10 vol. of buffered urea solution. Kinetic traces were fitted to double or triple exponential equations using Pro-Data Viewer software 4.2.12 (AP) to obtain relaxation rates and amplitudes.

FMN binding kinetics

The kinetics of FMN binding to WT, 3M and 6M apoflavodoxins at 25 °C was recorded following the quenching of FMN fluoresce

emission (excitation at 445 nm and emission beyond 500 nm). Equal volumes of protein (2 μM) and FMN (from 16 to 95 μM) solutions in 50 mM MOPS buffer, pH 7.0, were mixed in an AP SX17.MV stopped-flow apparatus. All data were analyzed with Pro-Data Viewer software 4.2.12 (AP) and fitted to either a single or a double exponential equation. Kinetic constants, k_{obs}, were plotted as functions of [FMN] in the mixture to calculate k_{on} values.

Thermal unfolding curves followed spectroscopically

Apoflavodoxin (40 μM in 50 mM MOPS pH 7.0) thermal unfolding[48,64] was monitored in the presence of 40 μM FMN following fluorescence emission (excitation at 280 nm; ratio of 320/360 nm emission) and near-UV CD (290 nm, 4 mm path length). The temperature was raised from 10 to 94 °C (at a rate of 1 °C min^{-1}). The curves for each variant were roughly normalized to values between 0 and 1 and globally fitted to a two-state model as previously described.[32]

Differential scanning calorimetry

Differential scanning calorimetry (DSC) measurements were performed from 10 to 110 °C, with a scanning rate of 1 °C min^{-1} on a high-precision VP-DSC differential scanning microcalorimeter (MicroCal LLC, Northampton, MA) using 40 μM protein solutions in 50 mM MOPS pH 7.0, with either 40, 80 or 160 μM FMN as described.[42] DSC data was analyzed using either a two-state model or a model-free analysis based on estimating overall parameters (namely, T_m, $\Delta H(T_m)$).

Equilibrium constants of the apoflavodoxin/FMN and flavodoxin/FNR complexes

The binding constants of the apoflavodoxin/FMN complexes have been determined at 25.0 ± 0.1 °C in 50 mM MOPS pH 7.0 essentially as previously described.[59] Small volume aliquots of apoflavodoxin were injected into a 0.5 μM FMN solution and fluorescence emission at 525 nm was recorded. The interaction between oxidized FNR and flavodoxin variants (1 : 1 apoflavodoxin/FMN complexes) was analyzed in 50 mM Tris/HCl pH 8.0 at 25.0 ± 0.1 °C by ITC, as described.[65] 20 μM FNR solutions were titrated with small volume aliquots of flavodoxin solutions using an automatic high-precision Auto-ITC200 system (MicroCal LLC, Northampton, MA). The binding parameters were estimated through nonlinear least squares regression using fitting routines developed by us, implemented in Origin (OriginLab).

Flavodoxin redox potentials

Midpoint reduction potentials, in 50 mM Tris/HCl pH 8.0 at 25 °C, for the ox/sq and sq/hq couples ($E_{ox/sq}$ and $E_{sq/hq}$ respectively) for WT flavodoxin and its 6M variant were determined in anaerobic conditions by potentiometric titration using photoreduction with a calomel electrode as a reference (E_m = 244.4 mV at 25 °C), as previously described.[50] The solution contained 40 μM flavodoxin, 1 mM EDTA, 1–2 μM deazariboflavin, and 1 μM of the following redox mediators: anthraquinone-2-sulfonate ($E_{m,pH\,7.0}$ = −225 mV for the determination of $E_{ox/sq}$), or benzyl viologen ($E_{m,pH\,7.0}$ = −359 mV) and methyl viologen ($E_{m,\ pH\,7.0}$ = −446 mV) for the determination of $E_{sq/hq}$. The midpoint potential of the redox couples were calculated by linear regression using the Nernst equation. Errors in the $E_{ox/sq}$ and $E_{sq/hq}$ determined were estimated to be ±5 mV.

Pre-steady-state electron transfer kinetics

Fast electron transfer from FNR_{hq} to Fld_{ox} was followed on an AP SX17. MV spectrophotometer using SX18.MV or Xscan software for experiments with single wavelength or photodiode-array detection, respectively. The experiments were carried out in 50 mM Tris/HCl, pH 8.0 at 12 °C, under anaerobic conditions obtained by several cycles of evacuation and bubbling with O_2-free argon.[66] FNR_{hq} samples were obtained by photoreduction in presence of 5 μM 5-deazariboflavin and 1 mM EDTA.[63] The two proteins were mixed (1 : 1) to final 10 μM concentrations. Spectral evolution was done by global analysis methods using the Pro-K software (AP). Data collected were fitted to a two-step model (A → B → C), with three spectral species representing distributions of enzyme intermediates (A: FNR_{hq} + Fld_{ox}, B: FNR_{sq} + Fld_{sq} + small amounts of FNR_{ox}, and C: Fld_{sq} + FNR_{ox}) along the reaction time course.[57]

X-ray structural determination of 6M (E20K/I59A/E72K/I92A/D126K/A142V) flavodoxin

Crystals were grown by the hanging drop vapor-diffusion method under conditions 26% PEG 4000 and 100 mM Tris/HCl, pH 8.0. Diffraction data were collected at 100 K on the BL13-XALOC at the ALBA (Spain) to a maximum resolution of 1.1 Å. The data set was processed with XDS[67] and scaled and reduced with SCALA.[68] The structure was solved using MOLREP[69] and the native *Anabaena* flavodoxin as model (pdb code 1FLV). REFMAC 5.0[70] and COOT[71] were used for automatic and manual refinement, respectively. The 6M flavodoxin model comprises residues 2–169, one FMN molecule, and 123 water molecules. Unit cell dimensions, other experimental data and refinement statistics are detailed in Table S4 (ESI†). Coordinates and structure factors are deposited in the PDB (5LJP).

Molecular dynamics simulations

200 ns-long MD simulations of WT and 6M flavodoxins (five replicas for each variant) were performed using the GROMACS 4.6.7 package,[72] with the CHARMM27 force field with CMAP correction (version 2.0),[73] using periodic boundary conditions and TIP3P[74] water molecules within a dodecahedron box of 5 nm of diameter. During the preparation step the systems were equilibrated at 300 K in an *NVT* (200 ps) and then in an *NPT* ensemble (500 ps) with a Berendsen barostat.[75] The Partial Mesh Ewald algorithm[76] was used to treat electrostatic interactions. For van der Waals interactions a cutoff method with the Potential-shift-Verlet modifier was used. Bond lengths were constrained using the LINCS algorithm,[77] and the time step was set to 2 fs. The trajectory files were analyzed using GROMACS' built-in functions to calculate root mean-square deviations (RMSD) and *B*-factors. Comparison of WT and 6M total volume was carried out, after having mutated the six

residues that differentiate the two proteins to alanine, using the web server 3vee.[78]

Author contributions

E. L. performed experiments and analyzed data, S. V. helped with performing experiments, A. V.-C., M. M.-J, J. J. G, P. F., and M. M. designed experiments and analyzed data, J. S. conceived the work, helped with performing experiments, analyzed data and wrote the manuscript. All authors reviewed the manuscript.

Competing financial interest

None.

Acknowledgements

This work was supported by Ministerio de Economía y Competitividad, Spain (grants BFU2013-47064-P, BIO2014-57314-REDT and BFU2016-78232-P) and Gobierno de Aragón, Spain (grant PI078/08 to Protein Targets B89).

References

1 Y. Bai, T. R. Sosnick, L. Mayne and S. W. Englander, *Science*, 1995, **269**, 192–197.
2 N. Cremades, J. Sancho and E. Freire, *Trends Biochem. Sci.*, 2006, **31**, 494–496.
3 D. D. Boehr, R. Nussinov and P. E. Wright, *Nat. Chem. Biol.*, 2009, **5**, 789–796.
4 M. H. Seo, J. Park, E. Kim, S. Hohng and H. S. Kim, *Nat. Commun.*, 2014, **5**, 3724.
5 P. Csermely, R. Palotai and R. Nussinov, *Trends Biochem. Sci.*, 2010, **35**, 539–546.
6 D. U. Ferreiro, J. A. Hegler, E. A. Komives and P. G. Wolynes, *Proc. Natl. Acad. Sci. U. S. A.*, 2011, **108**, 3499–3503.
7 P. I. Zhuravlev and G. A. Papoian, *Q. Rev. Biophys.*, 2010, **43**, 295–332.
8 S. J. Benkovic, G. G. Hammes and S. Hammes-Schiffer, *Biochemistry*, 2008, **47**, 3317–3321.
9 D. D. Boehr, D. McElheny, H. J. Dyson and P. E. Wright, *Science*, 2006, **313**, 1638–1642.
10 L. D. Antonov, S. Olsson, W. Boomsma and T. Hamelryck, *Phys. Chem. Chem. Phys.*, 2016, **18**, 5832–5838.
11 L. A. Campos, M. Bueno, J. Lopez-Llano, M. A. Jimenez and J. Sancho, *J. Mol. Biol.*, 2004, **344**, 239–255.
12 S. W. Englander, L. Mayne, Z. Y. Kan and W. Hu, *Annu. Rev. Biophys.*, 2016, **45**, 135–152.
13 I. Bahar, T. R. Lezon, L. W. Yang and E. Eyal, *Annu. Rev. Biophys.*, 2010, **39**, 23–42.
14 B. Rizzuti and V. Daggett, *Arch. Biochem. Biophys.*, 2013, **531**, 128–135.
15 U. Doshi, L. C. McGowan, S. T. Ladani and D. Hamelberg, *Proc. Natl. Acad. Sci. U. S. A.*, 2012, **109**, 5699–5704.
16 M. Tsytlonok and L. S. Itzhaki, *Arch. Biochem. Biophys.*, 2013, **531**, 14–23.
17 L. Carstensen, J. M. Sperl, M. Bocola, F. List, F. X. Schmid and R. Sterner, *J. Am. Chem. Soc.*, 2012, **134**, 12786–12791.
18 N. Ferguson, W. Li, A. P. Capaldi, C. Kleanthous and S. E. Radford, *J. Mol. Biol.*, 2001, **307**, 393–405.
19 B. K. Shoichet, W. A. Baase, R. Kuroki and B. W. Matthews, *Proc. Natl. Acad. Sci. U. S. A.*, 1995, **92**, 452–456.
20 K. E. Tang and K. A. Dill, *J. Biomol. Struct. Dyn.*, 1998, **16**, 397–411.
21 R. A. Goldstein, *Proteins*, 2011, **79**, 1396–1407.
22 D. M. Taverna and R. A. Goldstein, *Proteins*, 2002, **46**, 105–109.
23 M. J. Harms and J. W. Thornton, *Nat. Rev. Genet.*, 2013, **14**, 559–571.
24 T. Sikosek and H. S. Chan, *J. R. Soc., Interface*, 2014, **11**, 20140419.
25 I. F. Sevrioukova, *Antioxid. Redox Signaling*, 2011, **14**, 2545–2579.
26 D. Zhong, *Annu. Rev. Phys. Chem.*, 2015, **66**, 691–715.
27 K. S. Conrad, C. C. Manahan and B. R. Crane, *Nat. Chem. Biol.*, 2014, **10**, 801–809.
28 R. D. Ceccoli, D. A. Bianchi and D. V. Rial, *Front. Microbiol.*, 2014, **5**, 25.
29 W. P. Dijkman, G. de Gonzalo, A. Mattevi and M. W. Fraaije, *Appl. Microbiol. Biotechnol.*, 2013, **97**, 5177–5188.
30 R. D. Andersen, P. A. Apgar, R. M. Burnett, G. D. Darling, M. E. Lequesne, S. G. Mayhew and M. L. Ludwig, *Proc. Natl. Acad. Sci. U. S. A.*, 1972, **69**, 3189–3191.
31 K. D. Watenpaugh, L. C. Sieker, L. H. Jensen, J. Legall and M. Dubourdieu, *Proc. Natl. Acad. Sci. U. S. A.*, 1972, **69**, 3185–3188.
32 J. Sancho, *Cell. Mol. Life Sci.*, 2006, **63**, 855–864.
33 Q. Ye, Y. Hu and C. Jin, *PLoS One*, 2014, **9**, e103936.
34 Y. J. Bollen, A. H. Westphal, S. Lindhoud, W. J. van Berkel and C. P. van Mierlo, *Nat. Commun.*, 2012, **3**, 1010.
35 H. C. Chen and R. P. Swenson, *Biochemistry*, 2008, **47**, 13788–13799.
36 C. W. Chang, T. F. He, L. Guo, J. A. Stevens, T. Li, L. Wang and D. Zhong, *J. Am. Chem. Soc.*, 2010, **132**, 12741–12747.
37 S. Ayuso-Tejedor, V. E. Angarica, M. Bueno, L. A. Campos, O. Abian, P. Bernado, J. Sancho and M. A. Jimenez, *J. Mol. Biol.*, 2010, **400**, 922–934.
38 N. Cremades, A. Velazquez-Campoy, E. Freire and J. Sancho, *Biochemistry*, 2008, **47**, 627–639.
39 S. Ayuso-Tejedor, R. Garcia-Fandino, M. Orozco, J. Sancho and P. Bernado, *J. Mol. Biol.*, 2011, **406**, 604–619.
40 C. G. Genzor, A. Perales-Alcon, J. Sancho and A. Romero, *Nat. Struct. Biol.*, 1996, **3**, 329–332.
41 Y. J. M. Bollen, M. B. Kamphuis and C. P. M. van Mierlo, *Proc. Natl. Acad. Sci. U. S. A.*, 2006, **103**, 4095–4100.
42 E. Lamazares, I. Clemente, M. Bueno, A. Velazquez-Campoy and J. Sancho, *Sci. Rep.*, 2015, **5**, 9129.
43 L. A. Campos, M. M. Garcia-Mira, R. Godoy-Ruiz, J. M. Sanchez-Ruiz and J. Sancho, *J. Mol. Biol.*, 2004, **344**, 223–237.
44 M. Bueno, N. Cremades, J. L. Neira and J. Sancho, *J. Mol. Biol.*, 2006, **358**, 701–712.

45 J. Fernandez-Recio, C. G. Genzor and J. Sancho, *Biochemistry*, 2001, **40**, 15234–15245.
46 J. Lopez-Llano, S. Maldonado, S. Jain, A. Lostao, R. Godoy-Ruiz, J. M. Sanchez-Ruiz, M. Cortijo, J. Fernandez-Recio and J. Sancho, *J. Biol. Chem.*, 2004, **279**, 47184–47191.
47 M. Bueno, S. Ayuso-Tejedor and J. Sancho, *J. Mol. Biol.*, 2006, **359**, 813–824.
48 L. A. Campos and J. Sancho, *Proteins*, 2006, **63**, 581–594.
49 A. Lostao, F. Daoudi, M. P. Irun, A. Ramon, C. Fernandez-Cabrera, A. Romero and J. Sancho, *J. Biol. Chem.*, 2003, **278**, 24053–24061.
50 S. Frago, G. Goni, B. Herguedas, J. R. Peregrina, A. Serrano, I. Perez-Dorado, R. Molina, C. Gomez-Moreno, J. A. Hermoso, M. Martinez-Julvez, S. G. Mayhew and M. Medina, *Arch. Biochem. Biophys.*, 2007, **467**, 206–217.
51 X. Arias-Moreno, A. Velazquez-Campoy, J. C. Rodriguez, M. Pocovi and J. Sancho, *J. Biol. Chem.*, 2008, **283**, 22670–22679.
52 G. Goni, A. Serrano, S. Frago, M. Hervas, J. R. Peregrina, M. A. De la Rosa, C. Gomez-Moreno, J. A. Navarro and M. Medina, *Biochemistry*, 2008, **47**, 1207–1217.
53 J. K. Hurley, G. Tollin, M. Medina and C. Gómez-Moreno, in *The light-driven plastocyanin:ferredoxin oxidoreductase*, ed. J. H. Golbeck, Springer, Dordrecht, 2006, ch. 455, pp. 455–476.
54 M. Martinez-Julvez, M. Medina and A. Velazquez-Campoy, *Biophys. J.*, 2009, **96**, 4966–4975.
55 H. Bottin and B. Lagoutte, *Biochim. Biophys. Acta*, 1992, **1101**, 48–56.
56 G. Goni, B. Herguedas, M. Hervas, J. R. Peregrina, M. A. De la Rosa, C. Gomez-Moreno, J. A. Navarro, J. A. Hermoso, M. Martinez-Julvez and M. Medina, *Biochim. Biophys. Acta*, 2009, **1787**, 144–154.
57 A. Serrano and M. Medina, in *Advances in Photosynthesis – Fundamental Aspects*, ed. M. Najafpour, In Tech, 2012, DOI: 10.5772/19305.
58 J. Estrada, P. Bernado, M. Blackledge and J. Sancho, *BMC Bioinf.*, 2009, **10**, 104.
59 A. Lostao, M. El Harrous, F. Daoudi, A. Romero, A. Parody-Morreale and J. Sancho, *J. Biol. Chem.*, 2000, **275**, 9518–9526.
60 D. A. Hall, C. W. Vander Kooi, C. N. Stasik, S. Y. Stevens, E. R. Zuiderweg and R. G. Matthews, *Proc. Natl. Acad. Sci. U. S. A.*, 2001, **98**, 9521–9526.
61 M. Medina and C. Gomez-Moreno, *Photosynth. Res.*, 2004, **79**, 113–131.
62 C. G. Genzor, A. Beldarrain, C. Gomez-Moreno, J. L. Lopez-Lacomba, M. Cortijo and J. Sancho, *Protein Sci.*, 1996, **5**, 1376–1388.
63 M. Medina, M. Martinez-Julvez, J. K. Hurley, G. Tollin and C. Gomez-Moreno, *Biochemistry*, 1998, **37**, 2715–2728.
64 M. P. Irun, M. M. Garcia-Mira, J. M. Sanchez-Ruiz and J. Sancho, *J. Mol. Biol.*, 2001, **306**, 877–888.
65 A. Velazquez-Campoy, G. Goni, J. R. Peregrina and M. Medina, *Biophys. J.*, 2006, **91**, 1887–1904.
66 P. Ferreira, A. Hernandez-Ortega, B. Herguedas, A. T. Martinez and M. Medina, *J. Biol. Chem.*, 2009, **284**, 24840–24847.
67 W. Kabsch, *Acta Crystallogr., Sect. D: Biol. Crystallogr.*, 2010, **66**, 125–132.
68 P. Evans, *Acta Crystallogr., Sect. D: Biol. Crystallogr.*, 2006, **62**, 72–82.
69 A. A. Vagin and A. Teplyakov, *J. Appl. Crystallogr.*, 1997, **30**, 1022.
70 G. N. Murshudov, A. A. Vagin and E. J. Dodson, *Acta Crystallogr., Sect. D: Biol. Crystallogr.*, 1997, 240–255.
71 P. Emsley and K. Cowtan, *Acta Crystallogr., Sect. D: Biol. Crystallogr.*, 2004, **60**, 2126–2132.
72 D. Van Der Spoel, E. Lindahl, B. Hess, G. Groenhof, A. E. Mark and H. J. Berendsen, *J. Comput. Chem.*, 2005, **26**, 1701–1718.
73 A. D. J. MacKerell, M. Feig and C. L. Brooks, *J. Comput. Chem.*, 2004, **25**, 1400–1415.
74 W. L. Jorgensen, J. Chandrasekhar, J. D. Madura, R. W. Impey and M. L. Klein, *J. Chem. Phys.*, 1983, **79**, 926–935.
75 H. J. C. Berendsen, J. P. M. Postma, W. F. van Gunsteren, A. DiNola and J. R. Haak, *J. Chem. Phys.*, 1984, **81**, 3684–3690.
76 U. Essmann, L. Perera, M. L. Berkowitz, T. Darden, H. Lee and L. G. Pedersen, *J. Chem. Phys.*, 1995, **103**, 8577–8593.
77 B. Hess, H. Bekker, H. J. C. Berendsen and J. G. E. M. Fraaije, *J. Comput. Chem.*, 1997, **18**, 1463–1472.
78 R. V. Neil and M. Gerstein, *Nucleic Acids Res.*, 2010, **38**, W555–W562, web server issue.